Real-time broadening of nonequilibrium density profiles and the role of the specific initial-state realization

R. Steinigeweg,[1,*] F. Jin,[2] D. Schmidtke,[1] H. De Raedt,[3] K. Michielsen,[2,4] and J. Gemmer[1,†]

[1]*Department of Physics, University of Osnabrück, D-49069 Osnabrück, Germany*

[2]*Institute for Advanced Simulation, Jülich Supercomputing Centre, Forschungszentrum Jülich, D-52425 Jülich, Germany*

[3]*Zernike Institute for Advanced Materials, University of Groningen, NL-9747AG Groningen, The Netherlands*

[4]*RWTH Aachen University, D-52056 Aachen, Germany*

(Received 21 October 2016; published 31 January 2017)

The real-time broadening of density profiles starting from nonequilibrium states is at the center of transport in condensed-matter systems and dynamics in ultracold atomic gases. Initial profiles close to equilibrium are expected to evolve according to the linear response, e.g., as given by the current correlator evaluated exactly at equilibrium. Significantly off equilibrium, the linear response is expected to break down and even a description in terms of canonical ensembles is questionable. We unveil that single pure states with density profiles of maximum amplitude yield a broadening in perfect agreement with the linear response, if the structure of these states involves randomness in terms of decoherent off-diagonal density-matrix elements. While these states allow for spin diffusion in the XXZ spin-1/2 chain at large exchange anisotropies, coherences yield entirely different behavior.

DOI: 10.1103/PhysRevB.95.035155

I. INTRODUCTION

The mere existence of equilibration and thermalization is a key issue in many areas of modern many-body physics. While this question has a long and fertile history, it has experienced an upsurge of interest in recent years [1] due to the advent of cold-atomic gases [2] as well as the discovery of new states of matter such as many-body localized phases [3]. In particular, the theoretical understanding has seen substantial progress by the fascinating concepts of eigenstate thermalization [4–6] and typicality of pure quantum states [7–14], as well as by the invention of powerful numerical methods such as density-matrix renormalization group [15]. Much less is known on the route to equilibrium as such [16] and still the derivation of the conventional laws of (exponential) relaxation and (diffusive) transport on the basis of truly microscopic principles is a challenge to theory [17].

In strictly isolated systems, any coupling to heat baths or particle reservoirs and any driving by external forces is absent. In such systems, the only possibility to induce a nonequilibrium process is the preparation of a proper initial state. While different ways of preparation can be chosen, a sudden quench of the Hamiltonian is a common preparation scheme [18]. However, once a specific state is selected, a crucial question is the following: To what extent is this state a nonequilibrium state? To answer this question, it is natural to measure the observable one is interested in. If the expectation value is far from equilibrium, the state should be also. If this value is close to equilibrium, the state should be correspondingly. Moreover, only in the latter case, the resulting dynamics of the expectation value and linear response theory are expected to agree with each other. While this line of reasoning is certainly intuitive, it neglects internal degrees of freedom of the initial state. In particular, the measurement of a single observable cannot detect whether the underlying state is pure or mixed, entangled or nonentangled, etc. Therefore, an intriguing question is the following: Do such internal details play any role in the dynamics of an expectation value?

In this paper, we investigate exactly this question for the anisotropic spin-1/2 Heisenberg chain. Dynamics in this integrable many-body model has been under active scrutiny in various theoretical works and, in particular, spin dynamics constitutes a demanding problem resolved only partially despite much effort [19–40], even within the linear response regime and at high temperatures. While it has become clear that quasilocal conservation laws [25,26] necessarily lead to ballistic behavior below the isotropic point, numerical studies [36–39] have reported signatures of diffusion above this point, in agreement with perturbation theory [39] and classical simulations [40].

To investigate spin transport, we first introduce a class of pure initial states. These initial states feature identical density profiles, where a maximum δ peak is located in the middle of the chain and lies on top of a homogeneous background, similar to [38]. For a subclass with internal randomness, we then show analytically that the resulting nonequilibrium dynamics can be related to equilibrium correlation functions via the concept of typicality. This relation is verified, in addition, by large-scale numerical simulations. These numerical simulations also unveil the existence of remarkably clean diffusion for large exchange anisotropies, as one of our central findings. Eventually, we demonstrate that entirely different behavior emerges without any randomness in the initial state.

II. MODEL AND OBSERVABLES

The Hamiltonian of the XXZ spin-1/2 chain with periodic boundary conditions reads

$$H = J \sum_{r=1}^{L} \left(S_r^x S_{r+1}^x + S_r^y S_{r+1}^y + \Delta S_r^z S_{r+1}^z \right), \qquad (1)$$

*rsteinig@uos.de
†jgemmer@uos.de

where $S_r^{x,y,z}$ are spin-1/2 operators at site r, L is the number of sites, $J > 0$ is the antiferromagnetic exchange coupling constant, and $(\Delta - 1)$ is the anisotropy. For all parameters, this model is integrable in terms of the Bethe ansatz and the total magnetization $S^z = \sum_r S_r^z$ is a strictly conserved quantity. We take into account all subsectors of S^z, i.e., we consider the case $\langle S^z \rangle = 0$. We note that via the Jordan-Wigner transformation, this model can be mapped onto a chain of spinless fermions with particle interactions of strength Δ and total particle number $N = S^z + L/2$, i.e., $\langle N \rangle = L/2$ (see Appendix A for the half-filling case $N = L/2$).

We are interested in the nonequilibrium dynamics of the local occupation numbers $n_r = S_r^z + 1/2$. Specifically, we consider the expectation values $p_r(t) = \mathrm{tr}[n_r\, \rho(t)]$ for the density matrix $\rho(t)$ at time t. In this way, we study the time-dependent broadening of density profiles for a given initial state $\rho(0)$. In this paper, we focus on pure states $\rho(0) = |\psi(0)\rangle\langle\psi(0)|$.

III. INITIAL STATES

Obviously, it is possible to choose many different initial states $|\psi(0)\rangle$ and the resulting dynamics can depend on details of the specific choice. A frequently used preparation scheme is a quantum quench, i.e., $|\psi(0)\rangle$ is the eigenstate of another Hamiltonian. In this paper, however, we proceed in a different way.

To introduce our class of initial states, let $|\varphi_k\rangle$ be the common eigenbasis of all n_r, i.e., the Ising basis. Then, this class reads

$$|\psi(0)\rangle \propto n_{L/2}\,|\Phi\rangle, \quad |\Phi\rangle = \sum_{k=1}^{2^L} c_k\,|\varphi_k\rangle, \tag{2}$$

where c_k are complex coefficients and $n_{L/2}$ projects onto Ising states with a particle in the middle of the chain. By construction, $p_{L/2}(0) = 1$ is maximum.

In the above class, a particular state is the one where all c_k are the same. It yields $p_{r\neq L/2}(0) = p_{\mathrm{eq.}} = 1/2$ and still $p_{L/2}(0) = 1$. Hence, its density profile has a δ peak on top of a homogeneous background. However, the same density profile also results when the c_k are drawn at random according to the unitary invariant Haar measure [11] (where the real and imaginary parts of the c_k are drawn from a Gaussian distribution with zero mean, as done in our numerical simulations performed below). In other words, it is impossible to distinguish the two states with equal and random coefficients by a measurement of their initial density profiles $p_r(0)$ [41]. Only at times $t > 0$, their density profiles $p_r(t)$ can be different, if these density profiles differ at all. Note that similar $p_r(0)$ have been studied in Ref. [38].

Because our initial states are pure and have maximum $p_{L/2}(0) = 1$ as well, these states have to be considered as far-from-equilibrium states. Thus, it is natural to expect that the resulting dynamics of $p_r(t)$ cannot be described by linear response theory. However, such an expectation turns out to be wrong for the case of random c_k. In this case, $|\Phi\rangle$ is a typical state [7–14], i.e., a trace $\mathrm{tr}[\bullet]$ can be approximated by the expectation value $\langle\Phi|\bullet|\Phi\rangle$ with high accuracy in large Hilbert spaces. Using this fact and exact math (see Appendix B for more details), we find the relation

$$p_r(t) - p_{\mathrm{eq}} = 2\,\langle (n_{L/2} - p_{\mathrm{eq}})(n_r(t) - p_{\mathrm{eq}})\rangle, \tag{3}$$

where $\langle\bullet\rangle = \mathrm{tr}[\bullet]/2^L$. This relation is the first main result of our paper. It unveils that the expectation value $p_r(t)$ of a far-from-equilibrium state is directly connected to an equilibrium correlation function. It is important to note that such a relation cannot be derived for the other case of equal c_k (see also Appendix C for the specific type of randomness).

Due to the above relation, it is also possible to connect our nonequilibrium dynamics to the Kubo formula. To this end, one has to define the spatial variance,

$$\sigma(t)^2 = \sum_{r=1}^{L} r^2\,\delta p_r(t) - \left[\sum_{r=1}^{L} r\,\delta p_r(t)\right]^2, \tag{4}$$

with $\delta p_r(t) = 2[p_r(t) - p_{\mathrm{eq}}]$ and $\sum_{r=1}^{L} \delta p_r(t) = 1$. Then, following Ref. [42], it is straightforward to show that the time derivative of this variance,

$$\frac{d}{dt}\sigma(t)^2 = 2\,D(t), \tag{5}$$

is given by the time-dependent diffusion coefficient,

$$D(t) = \frac{4}{L}\int_0^t dt'\,\langle j(t')j\rangle, \tag{6}$$

where $j = \sum_{r=1}^{L} S_r^x S_{r+1}^y - S_r^y S_{r+1}^x$ is the well-known spin current. For $\Delta = 0$, $[j, H] = 0$ leads to $\mathcal{D}(t) \propto t$ such that $\sigma^2(t) \propto t^2$ scales ballistically. The partial conservation of j for $\Delta < 1$ [19–31] also excludes diffusive scaling $\sigma(t)^2 \propto t$ in this Δ regime. In fact, signatures of diffusion at high temperatures have been found only in the regime of large anisotropies, $\Delta > 1$ [36–39]. Note that $\sigma(t)^2 \propto t$ is merely a necessary and not sufficient criterion for diffusion since, by definition, the variance yields no information beyond the width of the distribution $\delta p_r(t)$. This is why we study the full space dependence. For a recent numerical survey of Eq. (5), see [43].

IV. NUMERICAL METHOD AND RESULTS

Numerically, the time evolution of a pure state $|\psi(t)\rangle$ can be calculated by the method of full exact diagonalization. But this method is restricted to $L \sim 20$ sites, even if symmetries such as the translation invariance of H are taken into account. Thus, we proceed differently and rely on a forward propagation of $|\psi(t)\rangle$ in real time. Such a propagation can be done by the use of fourth-order Runge-Kutta [14,30,31] or more sophisticated schemes such as Trotter decompositions or Chebyshev polynomials [44,45]. Here, we use a massively parallelized implementation of a Chebyshev-polynomial algorithm. In this way, we can treat system sizes as large as $L = 36$. For such L, we can guarantee that the initial δ peak is located sufficiently far from the boundary of the chain. Otherwise, we would have to deal with trivial finite-size effects and also Eq. (5) would not hold [42].

Next, we turn to our numerical results, starting with a typical initial state $|\psi(0)\rangle$, i.e., the case of random c_k. For a single realization of this state, we summarize in Fig. 1 the resulting expectation value $p_r(t)$ in a two-dimensional (2D) time-space density plot for different anisotropies, $\Delta = 1.5$,

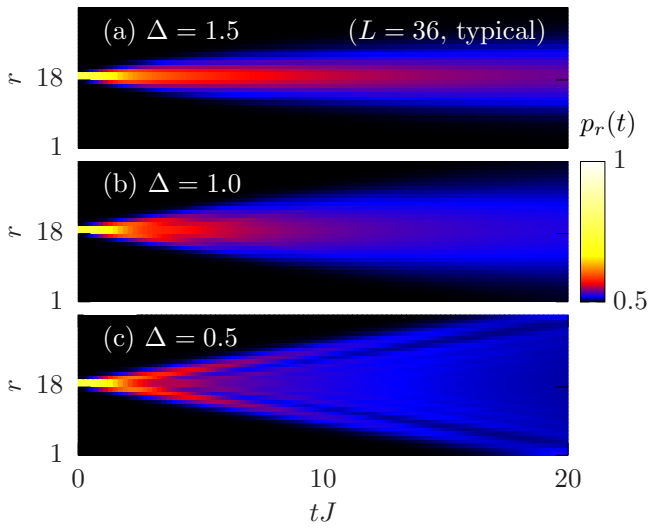

FIG. 1. Time-space density plot of occupation numbers $p_r(t)$ for a *typical* initial state $|\psi(0)\rangle$ in the XXZ spin-1/2 chain with $L = 36$ sites and different anisotropies: (a) $\Delta = 1.5$, (b) $\Delta = 1.0$, (c) $\Delta = 0.5$. The broadening in (a) is consistent with a diffusive process, while the broadening in (c) is ballistic.

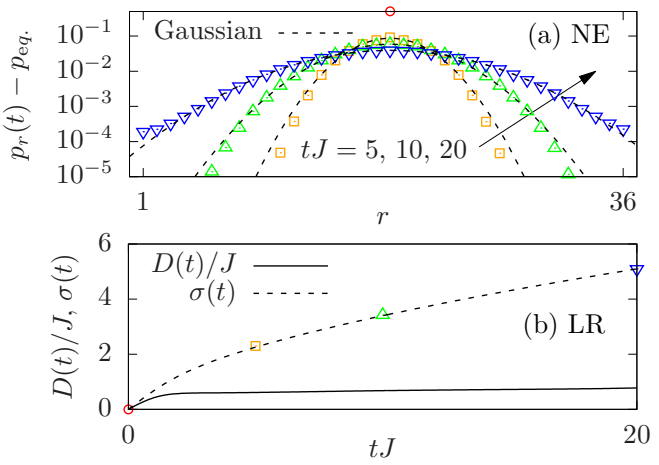

FIG. 2. (a) Density profile $p_r(t)$ with respect to site r at fixed times $tJ = 0$, 5, 10, 20 for a single anisotropy $\Delta = 1.5$ (and the parameters in Fig. 1), shown in a semilogarithmic plot (symbols). The indicated Gaussian fits describe the data very well over several orders of magnitude (curves). (b) Time dependence of diffusion coefficient $D(t)$ and profile width $\sigma(t)$ according to linear response theory, calculated in Ref. [31] for the same anisotropy $\Delta = 1.5$ and $L = 34$ sites (curves). For comparison, the standard deviation $\sigma(t)$ of the Gaussian fits in (a) is depicted (symbols).

1.0, 0.5, and a large system with $L = 36$ sites. Several comments are in order. First, for all values of Δ shown, the initial δ peak monotonously broadens as a function of time and the nonequilibrium density profiles have the irreversible tendency to equilibrate. Such equilibration is nontrivial in view of our isolated and integrable model. Second, for times below the maximum $tJ = 20$ depicted, the spatial extension of the density profiles is still smaller than the length of the chain. Thus, unwanted boundary effects do not emerge for such times. Third, the broadening of the density profiles is faster for smaller values of Δ because the scattering due to particle interactions decreases as Δ decreases. Moreover, for the small $\Delta = 0.5$ in Fig. 1(c), the width of the density profile clearly increases linearly as a function of time. This linear increase is the expected ballistic dynamics arising from partial conservation of the spin current. In contrast, for the larger $\Delta = 1.5$ and 1.0 in Figs. 1(a) and 1(b), the width of the density profiles does not increase linearly and is rather reminiscent of a square-root behavior. However, such a conclusion is not possible on the basis of a density plot.

To gain insight into the dynamics at $\Delta = 1.5$, we depict in Fig. 2(a) the site dependence of the expectation values $p_r(t)$ at fixed times $tJ = 0$, 5, 10, and 20. Conveniently, we subtract the equilibrium value p_{eq} and use a semilogarithmic plot to also visualize the tails of the density profiles. As illustrated by fits, the site dependence can be described by Gaussians [with $\sigma_{\mathrm{f}}(t)$ as the only fit parameter],

$$p_r(t) - p_{\mathrm{eq}} = \frac{1}{2}\,\frac{1}{\sqrt{2\pi}\,\sigma_{\mathrm{f}}(t)}\,\exp\left[-\frac{(r - L/2)^2}{2\,\sigma_{\mathrm{f}}(t)^2}\right], \qquad (7)$$

and, remarkably, over several orders of magnitude. Such a pronounced Gaussian form of the density profiles is the second main result of our paper. This result unveils that the standard deviation $\sigma_{\mathrm{f}}(t)$ is not just a width but also the only parameter required to describe the full site dependence. Furthermore, the Gaussian form is one of the clearest signatures of diffusion so far. Still, diffusion requires that $\sigma_{\mathrm{f}}(t)$ scales as $\sigma_{\mathrm{f}}(t) \propto \sqrt{t}$.

To further judge on diffusion, we show in Fig. 2(b) the standard deviation $\sigma_{\mathrm{f}}(t)$, as resulting from the Gaussian fits in Fig. 2(a). We further depict linear response results for $\sigma(t)$ in Eq. (5) and the underlying $D(t)$ in Eq. (6), as calculated in Ref. [31] for $L = 34 \sim 36$. On the one hand, the excellent agreement shows the very high accuracy of the typicality relation in Eq. (3). On the other hand, this agreement demonstrates that the known linear response result $\sigma(t) \propto \sqrt{t}$, resulting from $D(t) \approx \mathrm{const}$ at such t [31,38,39], also holds for our nonequilibrium density dynamics. Hence, together with the Gaussian form, we can conclude that diffusion exists.

An analogous analysis for the isotropic point $\Delta = 1.0$ in Fig. 3(a) shows that simple Gaussians are not able to describe the tails of the density profiles accurately. This is why the standard deviation $\sigma_{\mathrm{f}}(t)$ of the corresponding fits slightly deviates from the linear response result in Fig. 3(b). But these deviations disappear if $\sigma(t)$ is calculated exactly according to Eq. (4). Most notably, however, the time dependence of $\sigma(t)$ is inconsistent with diffusion, as can be seen most easily from the nonconstant $D(t)$. In fact, $\sigma(t)$ points to superdiffusion [37,40], contrary to [46].

Now, we turn to the untypical initial state $|\psi(0)\rangle$, i.e., the case of equal c_k. Recall that for this state, we obtain the same initial density profile but the relations in Eqs. (3) and (5) do not need to hold. In Fig. 4, we summarize the resulting expectation values $p_r(t)$ in a 2D time-space density plot again. Compared to Fig. 1, the broadening turns out to be clearly different. The dynamics is frozen for $\Delta = 1.5$ in Fig. 4(a) and features pronounced jets for $\Delta = 0.5$ in Fig. 4(c). In particular, we do not find obvious indications of equilibration, at least for all times considered. These observations constitute the third

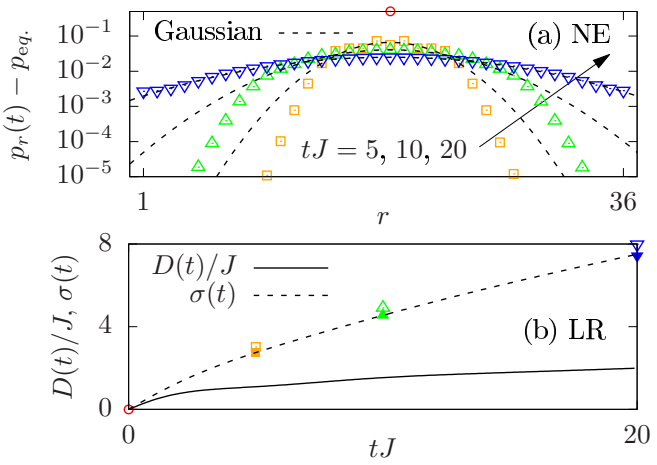

FIG. 3. The same data as depicted in Fig. 1 but now for the anisotropy $\Delta = 1.0$. In (a) the Gaussian fits cannot describe the tails of the density profiles accurately. In (b) the standard deviation of these fits (open symbols) and, according to Eq. (4) (closed symbols), still agrees with the linear response; however, the time dependence is clearly inconsistent with diffusion. Note that finite-size effects are negligibly small; see Appendix D.

main result of our paper. This result suggests that the lack of internal randomness in the initial condition is essential for the observation of nonequilibrium dynamics beyond linear response theory.

Finally, let us briefly mention another property of the untypical initial state $|\psi(0)\rangle$, which could be responsible for the special dynamics found. This property is the lack of entanglement. In fact, it is easy to see that $|\psi(0)\rangle$ can be written as the product state,

$$|\psi(0)\rangle \propto \cdots (|\uparrow\rangle + |\downarrow\rangle) \otimes |\uparrow\rangle \otimes (|\uparrow\rangle + |\downarrow\rangle) \cdots , \quad (8)$$

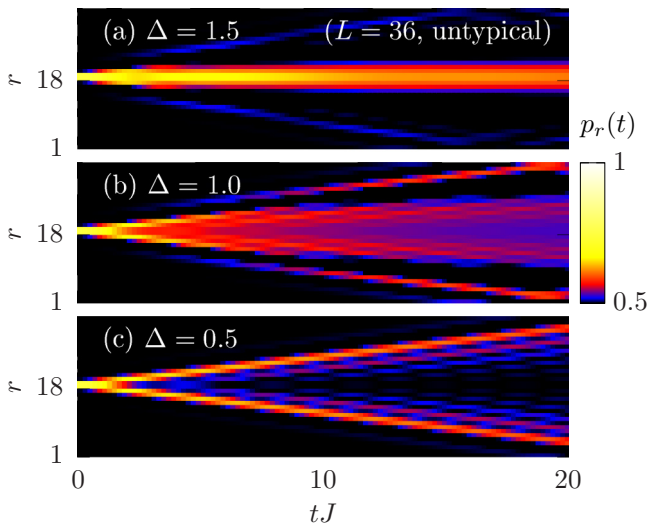

FIG. 4. Time-space density plot of occupation numbers $p_r(t)$ for another and *untypical* initial state $|\psi(0)\rangle$ in the XXZ spin-1/2 chain with $L = 36$ sites and different anisotropies: (a) $\Delta = 1.5$, (b) $\Delta = 1.0$, (c) $\Delta = 0.5$. Compared to Fig. 1, the dynamics is frozen in (a), similar to [33], and features pronounced jets in (c).

with a spin-up state $|\uparrow\rangle$ in the middle of the chain and a spin-up/spin-down superposition $|\uparrow\rangle + |\downarrow\rangle$ at all other sites. By definition, such a product state is not entangled at all. In clear contrast, the typical initial state cannot be written as a product state.

V. CONCLUSIONS

In this paper, we have investigated the real-time broadening of nonequilibrium density profiles in the spin-1/2 XXZ chain. First, we have introduced a class of pure initial states with identical density profiles where a maximum δ peak is located in the middle of the chain. Then, we have shown for a subclass with internal randomness that the resulting nonequilibrium dynamics can be connected to equilibrium correlation functions via the concept of typicality. This analytical result has also been verified by large-scale numerical simulations. These numerical simulations have further unveiled the existence of diffusion for large exchange anisotropies, as one of our key results. Finally, we have demonstrated that entirely different behavior emerges without any randomness in the initial state. Promising future directions of research include the identification of typical and untypical initial states in nonintegrable models, in many-body localized phases, and at low temperatures, as well as a systematic analysis of the role of entanglement.

ACKNOWLEDGMENTS

We sincerely thank T. Prosen and F. Heidrich-Meisner for fruitful discussions. In addition, we gratefully acknowledge the computing time, granted by the "JARA-HPC Vergabegremium" and provided on the "JARA-HPC Partition" part of the supercomputer "JUQUEEN" [47] at Forschungszentrum Jülich.

APPENDIX A: HALF-FILLING SECTOR

To demonstrate that our results do not depend on our specific choice of $\langle S^z \rangle = 0$, we do the calculation in, e.g., Fig. 4 again for the half-filling sector $S^z = 0$. We depict the corresponding results in Fig. 5. It is clearly visible that the real-time broadening of the expectation values $p_r(t)$ is practically the same, apart from minor details related to $p_{eq} \approx 1/2$ in the half-filling case.

APPENDIX B: TYPICALITY APPROXIMATION

Here, we provide details on the calculation leading to the relation in Eq. (3) of the main text. By carrying out the multiplication of the two brackets in the correlation function,

$$C(t) = 2\,\langle (n_{L/2} - p_{eq})(n_r(t) - p_{eq}) \rangle + p_{eq}, \quad (B1)$$

and applying $\langle n_r(t) \rangle = p_{eq}$, we obtain

$$C(t) = 2\,\langle n_{L/2}\, n_r(t) \rangle = 2\,\frac{\mathrm{tr}[n_{L/2}\, n_r(t)]}{2^L}. \quad (B2)$$

Using $n_{L/2}^2 = n_{L/2}$ and a cyclic permutation in the trace, we get

$$C(t) = 2\,\frac{\mathrm{tr}[n_{L/2}\, n_r(t)\, n_{L/2}]}{2^L}. \quad (B3)$$

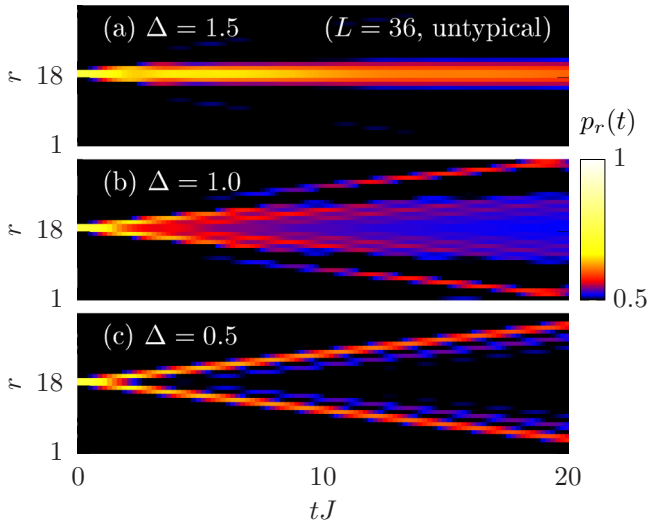

FIG. 5. The same data as shown in Fig. 4, but now for the half-filling sector $S^z = 0$.

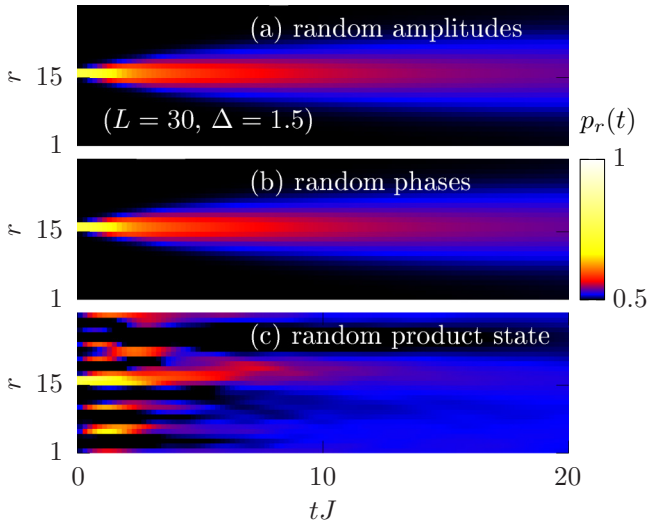

FIG. 6. Time-space density plot of occupation numbers $p_r(t)$ in the spin-1/2 XXZ chain with $L = 30$ sites and a single anisotropy $\Delta = 1.5$ for three different types of randomness in the pure initial state: (a) random amplitudes, (b) random phases, (c) random product state. See text for the detailed definitions.

Exploiting the typicality of the pure state $|\Phi\rangle$, the correlation function can be rewritten as

$$C(t) = 2\,\frac{\langle\Phi|\, n_{L/2}\, n_r(t)\, n_{L/2}\,|\Phi\rangle}{\langle\Phi|\Phi\rangle} + \epsilon, \tag{B4}$$

with the small error $\epsilon \propto 2^{-L/2}$. Due to $n_{L/2}^{\dagger} = n_{L/2}$, this expression becomes

$$C(t) = 2\,\frac{\langle n_{L/2}\,\Phi|\, n_r(t)\,|n_{L/2}\,\Phi\rangle}{\langle\Phi|\Phi\rangle} + \epsilon, \tag{B5}$$

and, due to $n_r(t) = e^{\imath Ht}\, n_r\, e^{-\imath Ht}$, it reads

$$C(t) = \frac{\langle e^{-\imath Ht}\, n_{L/2}\,\Phi|\, n_r\,|e^{-\imath Ht}\, n_{L/2}\,\Phi\rangle}{\langle\Phi|\Phi\rangle/2} + \epsilon, \tag{B6}$$

where we have moved, in addition, the factor 2 from the front to the denominator. Finally, due to the definition of $|\psi(0)\rangle$, we can write

$$C(t) = \langle\psi(t)|\, n_r\,|\psi(t)\rangle + \epsilon = p_r(t) + \epsilon. \tag{B7}$$

Therefore, comparing Eqs. (B1) and (B7) and skipping the small error ϵ for clarity yields

$$p_r(t) - p_{\mathrm{eq}} = 2\,\langle (n_{L/2} - p_{\mathrm{eq}})(n_r(t) - p_{\mathrm{eq}})\rangle. \tag{B8}$$

APPENDIX C: SPECIFIC TYPE OF RANDOMNESS

As stated in the main text, the relations in Eqs. (3) and (5) have to be understood for typical states $|\Phi\rangle$ drawn at random according to the unitary invariant Haar measure (where the real and imaginary parts of the c_k are drawn from a Gaussian distribution with zero mean). However, it is instructive to consider other types of randomness. Thus, we choose

$$c_k \propto e^{\imath\,\alpha_k}, \tag{C1}$$

with constant amplitudes $|c_k|^2$ and random phases α_k drawn from a uniform distribution $[0, 2\pi]$. In Figs. 6(a) and 6(b), we compare the resulting real-time broadening of the expectation values $p_r(t)$ for this and the previous choice of the c_k, where we focus on a single anisotropy $\Delta = 1.5$ and restrict ourselves to a chain length $L = 30$ to reduce computational effort. The excellent agreement demonstrates that the specific type of randomness does not matter. Moreover, constant amplitudes $|c_k|^2$ as such are not responsible for the untypical dynamics observed in Fig. 4.

Note that not any kind of randomness can yield the same dynamical behavior. To illustrate this fact, let us randomize the product state in Eq. (8) of the main text in the following way: At all sites $r \neq L/2$, we replace the spin-up/spin-down superposition $|\uparrow\rangle + |\downarrow\rangle$ by

$$e^{\imath\,\alpha_r}\,|\uparrow\rangle + e^{\imath\,\beta_r}\,|\downarrow\rangle, \tag{C2}$$

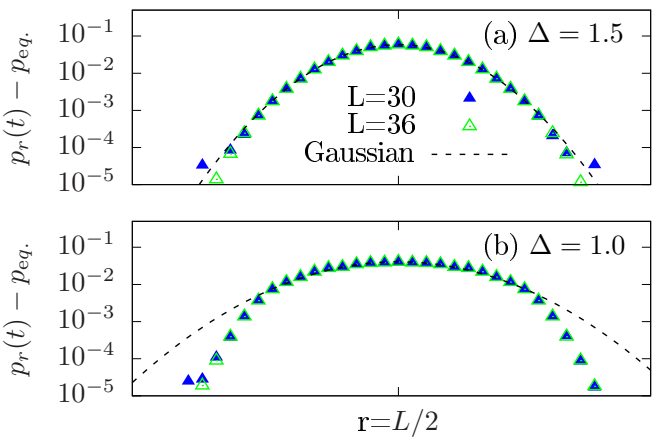

FIG. 7. Density profile $p_r(t)$ with respect to site r at a single time $tJ = 10$ for the two system sizes $L = 30$ and $L = 36$ and for the two anisotropies (a) $\Delta = 1.5$ and (b) $\Delta = 1.0$ (symbols). Gaussian fits are indicated for comparison (curves).

with site-dependent phases α_r, β_r drawn from a uniform distribution $[0,2\pi]$. This randomized product state has still $p_{r\neq L/2}(0) = 1/2$ and $p_{L/2}(0) = 1$. It involves only $2(L-1)$ random numbers, in contrast to the state from the Haar measure with 2^L random numbers. In Fig. 6(c), we depict the resulting dynamics of the expectation values $p_r(t)$. Compared to the two other random cases in Figs. 6(a) and 6(b), the dynamical behavior turns out to be very different. This difference suggests again that the lack of entanglement could be the source of untypical dynamics.

APPENDIX D: FINITE-SIZE EFFECTS

Eventually, we show that our numerical results for the real-time broadening of the expectation values $p_r(t)$ are free of significant finite-size effects. To this end, we redo the $t\,J = 10$ calculations in Figs. 2(a) and 3(a) for a smaller but still large system size $L = 30$. In Fig. 7, we depict the results of these calculations, together with the previous $L = 36$ data. It is clearly visible that finite-size effects are negligibly small and are not responsible for the non-Gaussian tails at the isotropic point $\Delta = 1.0$.

[1] J. Eisert, M. Friesdorf, and C. Gogolin, Nat. Phys. **11**, 124 (2015).
[2] T. Langen, R. Geiger, and J. Schmiedmayer, Annu. Rev. Condens. Matter Phys. **6**, 201 (2015).
[3] R. Nandkishore and D. A. Huse, Annu. Rev. Condens. Matter Phys. **6**, 15 (2015).
[4] J. M. Deutsch, Phys. Rev. A **43**, 2046 (1991).
[5] M. Srednicki, Phys. Rev. E **50**, 888 (1994).
[6] M. Rigol, V. Dunjko, and M. Olshanii, Nature (London) **452**, 854 (2008).
[7] J. Gemmer and G. Mahler, Eur. Phys. J. B **31**, 249 (2003).
[8] S. Goldstein, J. L. Lebowitz, R. Tumulka, and N. Zanghì, Phys. Rev. Lett. **96**, 050403 (2006).
[9] S. Popescu, A. J. Short, and A. Winter, Nat. Phys. **2**, 754 (2006).
[10] P. Reimann, Phys. Rev. Lett. **99**, 160404 (2007).
[11] C. Bartsch and J. Gemmer, Phys. Rev. Lett. **102**, 110403 (2009); Europhys. Lett. **96**, 60008 (2011).
[12] S. Sugiura and A. Shimizu, Phys. Rev. Lett. **108**, 240401 (2012).
[13] S. Sugiura and A. Shimizu, Phys. Rev. Lett. **111**, 010401 (2013).
[14] T. A. Elsayed and B. V. Fine, Phys. Rev. Lett. **110**, 070404 (2013).
[15] U. Schollwöck, Rev. Mod. Phys. **77**, 259 (2005); Ann. Phys. **326**, 96 (2011).
[16] P. Reimann, Nat. Commun. **7**, 10821 (2016).
[17] M. Buchanan, Nat. Phys. **1**, 71 (2005).
[18] F. H. L. Essler and M. Fagotti, J. Stat. Mech. Theor. Exp. (2016) 064002.
[19] B. S. Shastry and B. Sutherland, Phys. Rev. Lett. **65**, 243 (1990).
[20] B. N. Narozhny, A. J. Millis, and N. Andrei, Phys. Rev. B **58**, R2921 (1998).
[21] X. Zotos, Phys. Rev. Lett. **82**, 1764 (1999).
[22] J. Benz, T. Fukui, A. Klümper, and C. Scheeren, J. Phys. Soc. Jpn. **74**, 181 (2005).
[23] F. Heidrich-Meisner, A. Honecker, D. C. Cabra, and W. Brenig, Phys. Rev. B **68**, 134436 (2003).
[24] S. Fujimoto and N. Kawakami, Phys. Rev. Lett. **90**, 197202 (2003).
[25] T. Prosen, Phys. Rev. Lett. **106**, 217206 (2011).
[26] T. Prosen and E. Ilievski, Phys. Rev. Lett. **111**, 057203 (2013).
[27] J. Herbrych, P. Prelovšek, and X. Zotos, Phys. Rev. B **84**, 155125 (2011).
[28] C. Karrasch, J. H. Bardarson, and J. E. Moore, Phys. Rev. Lett. **108**, 227206 (2012).
[29] C. Karrasch, J. Hauschild, S. Langer, and F. Heidrich-Meisner, Phys. Rev. B **87**, 245128 (2013).
[30] R. Steinigeweg, J. Gemmer, and W. Brenig, Phys. Rev. Lett. **112**, 120601 (2014).
[31] R. Steinigeweg, J. Gemmer, and W. Brenig, Phys. Rev. B **91**, 104404 (2015).
[32] J. M. P. Carmelo, T. Prosen, and D. K. Campbell, Phys. Rev. B **92**, 165133 (2015).
[33] D. Gobert, C. Kollath, U. Schollwöck, and G. Schütz, Phys. Rev. E **71**, 036102 (2005).
[34] J. Sirker, R. G. Pereira, and I. Affleck, Phys. Rev. Lett. **103**, 216602 (2009); Phys. Rev. B **83**, 035115 (2011).
[35] S. Grossjohann and W. Brenig, Phys. Rev. B **81**, 012404 (2010).
[36] P. Prelovšek, S. El Shawish, X. Zotos, and M. Long, Phys. Rev. B **70**, 205129 (2004).
[37] M. Žnidarič, Phys. Rev. Lett. **106**, 220601 (2011).
[38] C. Karrasch, J. E. Moore, and F. Heidrich-Meisner, Phys. Rev. B **89**, 075139 (2014).
[39] R. Steinigeweg and W. Brenig, Phys. Rev. Lett. **107**, 250602 (2011).
[40] R. Steinigeweg, Europhys. Lett. **97**, 67001 (2012).
[41] Strictly speaking, by drawing c_k at random, it is possible to get the outcome $c_k = \text{const}$ for all $k = 1,\ldots,2^L$.
[42] R. Steinigeweg, H. Wichterich, and J. Gemmer, Europhys. Lett. **88**, 10004 (2009).
[43] C. Karrasch, T. Prosen, and F. Heidrich-Meisner, arXiv:1611.04832.
[44] R. Steinigeweg, F. Heidrich-Meisner, J. Gemmer, K. Michielsen, and H. De Raedt, Phys. Rev. B **90**, 094417 (2014).
[45] F. Jin, R. Steinigeweg, F. Heidrich-Meisner, K. Michielsen, and H. De Raedt, Phys. Rev. B **92**, 205103 (2015).
[46] I. Khait, S. Gazit, N. Y. Yao, and A. Auerbach, Phys. Rev. B **93**, 224205 (2016).
[47] M. Stephan and J. Docter, J. Large-Scale Res. Facil. **A1**, 1 (2015).